Optical Engineering

SPIEDigitalLibrary.org/oe

Measurement of helicopter rotor blade deformation using digital image correlation

Jayant Sirohi
Michael S. Lawson

Optical Engineering 51(4), 043603 (April 2012)

Measurement of helicopter rotor blade deformation using digital image correlation

Jayant Sirohi
Michael S. Lawson
The University of Texas at Austin
Department of Aerospace Engineering and Engineering Mechanics
Austin, Texas 78712
E-mail: jayant.sirohi@mail.utexas.edu

Abstract. An experimental study on the application of the digital image correlation (DIC) technique to measure the deformation of rotating helicopter blades is described. Measurements on two different rotors of diameter 24 and 39 in., with different rotor hubs, were carried out to explore applicability of the technique over a range of scales. Commercial DIC software was synchronized with the frequency of rotation such that rotor blade images could be obtained at a constant rotor azimuth. Bending and torsion mode shapes were extracted from the data with deformation as high as 0.4 in. measured with an accuracy of 0.0038 in. This technique is very advantageous because it is noncontact, cost effective, accurate and simple to implement while yielding full-field, three-dimensional data with a high spatial resolution. [DOI: 10.1117/1.OE.51.4.043603]

Subject terms: digital image correlation; rotorcraft; helicopter blade deformation; optical methods.

Paper 111463 received Nov. 22, 2011; revised manuscript received Feb. 7, 2012; accepted for publication Feb. 17, 2012; published online Apr. 6, 2012.

1 Introduction

Helicopter rotor blades typically are long, slender and flexible structures. They are subjected to unsteady aerodynamic loads as well as inertial loads due to blade motion. As a consequence, helicopter rotor blades undergo large deflections out of the rotor disk plane (flapping), in the rotor disk plane (lead-lag) and torsion along the blade span. Due to the presence of articulation at the rotor hub, the deflection of a rotor blade may be comprised of rigid body rotations about the blade root in addition to bending and twist deformation. Measurement of these rigid body rotations as well as the blade deformations, is important for a variety of purposes. For example, this data can be used to validate analyses that predict the performance and vibration of helicopters. Real-time blade deformation data can also be used for health monitoring of the rotor and sensory feedback for active vibration reduction systems.

Robust and reliable measurement of rotating blade deformation is very challenging. Electrical signals from sensors on the rotating frame must be transferred to the fuselage through an electrical slip ring. While rigid body rotations at the blade root can be measured by discrete sensors, such as potentiometers, measurement of blade bending and twist deformation requires distributed sensors along the rotor blade. Typically, strain gauges bonded to the blade at discrete span-wise locations are used to measure blade bending and twist. However, this approach has several drawbacks. The limited number of strain gauge locations results in a low spatial resolution of the measurements. The lack of deformation data over the entire blade span has led to the use of assumed deformations and interpolated data for the validation of aerodynamic analyses.[1,2] Because signal conditioning electronics are located in the fixed frame, the small imbalance voltage signal of the Wheatstone bridge has to be transmitted through an electric slip ring. This results in a poor signal to noise ratio. The strain gauge installations are easily damaged and it is not uncommon for several strain gauges to fail during wind tunnel or flight testing. Finally, each new rotor blade requires an elaborate installation procedure for the strain gauges which can be time consuming and costly over the course of a test program. These issues are exacerbated in the case of reduced-scale rotor testing, where there is less area available for application of the gauges and the centrifugal loads on the blades are much higher due to the increased tip speeds (see Fig. 1). For multiple channels of strain gauge data, the size of the slip ring becomes prohibitive considering the reduced size of the test article.

For these reasons, optical methods of measuring rotor blade deformation are very attractive. The major advantages of optical techniques are that they are noncontact and do not require extensive instrumentation of the structure. They do not require electrical slip rings and different test articles can be tested in the same measurement setup with minimal preparation. There have been several studies on measuring rotating blade deformation using optical techniques such as photogrammetry and projection moiré interferometry (PMI). This paper describes the use of the stereoscopic three-dimensional (3-D) digital image correlation (DIC) technique to measure deformation on reduced-scale helicopter rotor blades under static and dynamic loads. The technique is validated by comparing results obtained by a laser displacement sensor (LDS) on a vibrating beam. The goal is to offer a full-field alternative for strain measurement of rotor blades that provides superior resolution over traditional strain gauges and is cost effective, accurate, and simple to implement.

2 Optical Deformation Measurement Techniques

Optical full-field measurement techniques have, over the course of the past few decades, grown increasingly useful

0091-3286/2012/$25.00

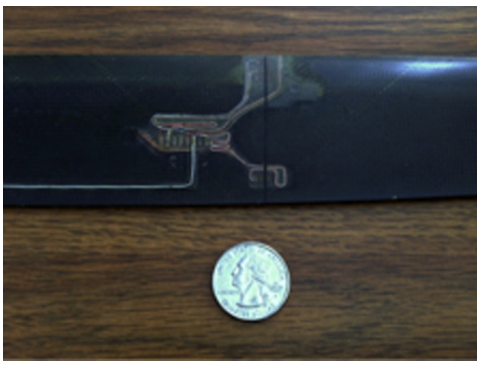

Fig. 1 Strain gauge installation on a 0.15 scale Bell 412 Helicopter rotor blade.

in engineering research and development to help facilitate design, materials production, and inspection.[3] Holographic interferometry (HI), electronic speckle pattern interferometry (ESPI), Moiré techniques, and DIC technique have been thoroughly explored from theoretical[4,5] and engineering application[6,7] viewpoints. It may be remarked that both ESPI and HI possess high sensitivity but have limited range. DIC extends this range by several orders of magnitude.[8]

There has been some limited investigation of optical measurement techniques for helicopter rotor blade deformation. Flemming and Gorton[9] used PMI to obtain 3-D deformation measurements of rotor blades and demonstrated the superior attributes of the technique compared to conventional approaches. The technique was also applied to characterize the vibrations of a NASA active twist rotor blade.[10] PMI relies on the projection of equally spaced grid on the model surface. The image of the model surface overlaid with grid lines is superposed on the computer generated reference grid, resulting in moiré fringe formation. Moiré fringe pattern is analyzed using computational phase-shifting technique to obtain shape and deformation of the object. Olson et al.[11] used photogrammetry to measure the deformation of full-scale UH-60 helicopter blades in a wind tunnel at various wind speeds, rotor thrusts, and drive shaft angles. This technique used 2 in. diameter reflective, circular targets attached at specific locations on the blade. The experimental setup was calibrated using the known positions of targets mounted on the wind tunnel walls. The measured deformation and twist distribution closely matched expected values. There have been several other studies using photogrammetry for visualizing structural deformation and also to maintain productivity.[12–14]

Previous studies have provided a solid foundation for the advancement of the DIC technique since the early 1980s.[15] The technique has been extensively used in material sciences and biomedical engineering to measure deformations in a variety of systems such as high speed fracture and rotating flywheels,[16] deformations in flapping wings for a micro-aerial vehicle,[17] tensile test of a knee tendon,[18] dynamic tissue deformation measurements of a frog heart and of artificial muscles. Kahn-Jetter and Chu[19] presented an overview of DIC theory with experimental verification on a cantilever beam, as well as a brief discussion on methods of random speckle pattern and photogrammetric principles. They concluded that the technique is viable for determining 3-D displacements. The effect of camera tilt is negligible and increasing the camera magnification improves the results. McNeill et al.[20] discussed the differences between several DIC approaches and calibration methods. Several studies have addressed the advantages of using DIC over single-point conventional strain gauges. For example, Siebert et al.[21] measured the strain at three points on a vibrating cantilever beam using conventional strain gauges and compared the results to the strain measured using DIC.

There are several benefits to using DIC to measure rotor blade deformation. Most important is the fact that single-point strain gauges are incapable of showing strain gradients and could potentially miss high strain hot spots, whereas DIC yields measurements with a very high spatial resolution, on the order of $1/30,000$ of the field of view.[3] The output of the DIC technique is a deformation map, which can be used to quickly verify finite element models. DIC does not require involved sample preparation or the installation of electronic slip rings. DIC can also be applied to small or complex geometry, where it is challenging to install conventional strain gauges. Because DIC does not require instrumentation exposed to the high vibration environment on the rotor blades, it is a more robust technique than strain gauges. Additionally, DIC is not affected by rigid body motions and can measure large deformations as long as the test object remains within focus of the cameras.

3 DIC Technique

In the DIC technique, the surface of the model is painted with a random dot or "speckle" (salt and pepper) pattern. A convenient method to create such a pattern is to paint the surface with a matte background color and spray it with a high-contrast color. A high-resolution camera captures images of the surface before and after deformation. Cross-correlation of these images yields a two-dimensional (2-D), or in-plane, displacement map of the surface.

This technique can be extended to three dimensions by incorporating photogrammetric principles. In three-dimensional DIC, two high-resolution cameras are separated by a fixed distance and arranged so that they view the same area on the test article (Fig. 2). The surface height of a particular point on the surface of the test article can be determined from the parallax, or stereoscopic disparity between the two camera images. The experimental setup must be calibrated to calculate the mapping function between physical dimensions on the test article and the corresponding parallax

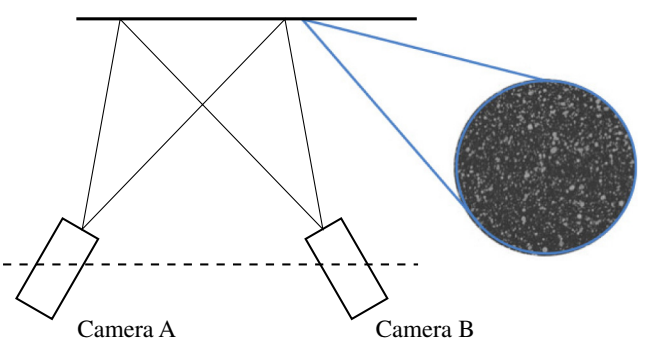

Fig. 2 Typical stereoscopic DIC setup with speckle pattern on test article.

on the image plane of the cameras. This calibration is performed using a target of known geometry. After this mapping function is generated, any length on the image plane can be converted to physical dimensions using photogrammetry. Note that the use of parallax enables 3-D displacements to be measured. The geometric arrangement of the cameras and test article must remain undisturbed for the duration of the experiment to ensure the validity of the mapping function. Cross-correlation of images before and after deformation of the test article, in conjunction with the parallax mapping function, yields a 3-D map of the surface. Comparing this map to a reference undeformed surface yields a displacement, or deformation map, of the test article.

The calibration of the test setup, as well as the surface height determination are crucial steps in measuring the deformation using DIC. These steps are described below.

3.1 *Test Setup Calibration*

Calibration defines an internal representation of the position and orientation of the cameras relative to the sample. The calibration (expressed, for example, in pixel/mm), represents a mapping between the camera image planes and real world dimensions. Measurements in three dimensions require a calibration in multiple planes; so a polynomial calibration, which uses either a 3-D calibration plate or multiple coplanar views of a 2-D calibration plate, is required. A 3-D calibration plate was used in the present set of experiments. It is not necessary for the calibration plate to be aligned exactly with respect to the test article or the cameras. This allows the target to be held by hand in front of the test article, and thus, considerably simplifies the calibration process. After capturing several images, the distinct marks on the calibration target must be manually identified in the software, which then calculates the mapping function.

3.2 *Surface Height Calculation*

The first step in the surface height calculation is to define a mask that will exclude any background pixels that are not a part of the test article. The mask can be geometrically fixed for all images; a moving mask fixed to structures, or algorithmically determined based on intensity counts for all images in the set.

Given a pair of camera images, the surface height of the test article can be calculated by identifying groups of pixels in both images and using the mapping functions that were defined during the camera calibration process. This process is shown in Fig. 3. The test article is indicated by the grey rectangle in image A and image B from camera 1 and camera 2, respectively. The area of interest is divided into a rectangular grid with a given number of pixels grouped together in each element (called interrogation window). For example, each group can be of size 16×16 pixels or 4×4 pixels, and a single point is associated with the center of the interrogation window. The corresponding points (x_1, y_1) and (x_2, y_2) from the two cameras are found by cross-correlation of the images A and B. By passing the x and y coordinates through the mapping function $H(x, y)$, the height of each representative point (corresponding to a group of pixels) can be determined by an iterative process to create a surface of the test article. This process is repeated for every pair of images in a set of recorded images. This has to be done very carefully for the first image in the set; however, subsequent

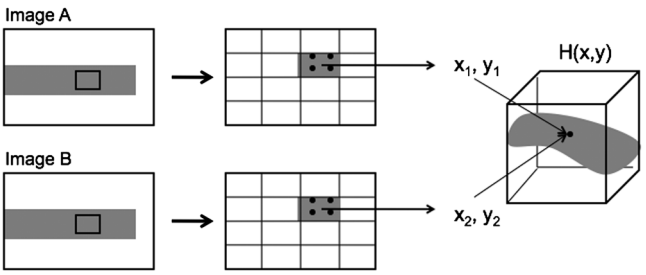

Fig. 3 Calculation of surface height by cross-correlation of camera images followed by photogrammetry.

images can use the result of the first (or preceding) image as the initial guess. This implies that the deformation is small enough that consecutive surfaces do not change substantially, though it is possible to calculate each surface from generalized settings, this takes much more time to compute.

3.3 *Displacement Calculation*

Once the test article surface is calculated for all images in a set, a vector deformation field can be calculated by comparing each surface to a baseline or reference surface (Fig. 4). Typically, the reference surface is in the unloaded, or undeformed, condition while subsequent surfaces are calculated after the test article has been loaded, or deformed. A variety of post processing options are possible including eliminating vectors that are not consistent or differ from their neighboring vectors by a specified factor, inserting vectors in empty spots in the vector field, and smoothing.

4 Experimental Setup and Test Procedure

The cameras (Imager ProX 2M) used for these experiments have a 1600×1200 pixel resolution, 29.5 Hz operation speed (15 Hz continuous), color CCD image sensors, internal camera memory, and 16384 (14-bit) gray levels. The exposure time is adjustable within the range of 500 ns to 1000 ms and the cameras are capable of accepting an auxiliary TTL triggering signal. The cameras were equipped with Nikon 50 mm AF NIKKOR $f/1.8$D lenses; these lenses do not have any zoom control and a minimum focal distance of 1.5 ft (0.45 m), though they have a variable aperture from f1.8 to f22. The DIC software used was Lavision DaVis 7.2-StrainMaster 3-D.[22]

The surfaces were prepared by applying a matte black or white coat of paint followed by a speckle pattern of opposite color; the speckle pattern was applied either by using a toothbrush dipped in the paint and flicking it over the sample or by spraying a light coat from a distance. It was observed

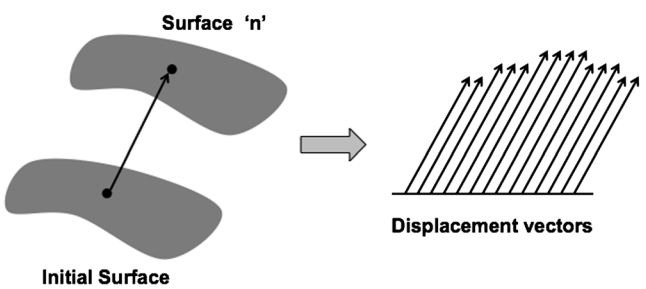

Fig. 4 Calculation of vector displacement field by comparing deformed test article surface "*n*" to initial test article surface.

that using black speckles on a matte white coat was easier to work with, as the image would have higher intensity and better contrast with the background.

In all the experiments, a set of image frames was captured at the same point in the period of motion, so that the image would appear motionless. The surface height was then calculated for each image in the set based on a mask, and various iterative calculation parameters and postprocessing parameters. Finally, the surface heights for each image in the set were compared to a reference surface and the surface, deformation was calculated. This surface deformation was then be exported and analyzed independent from the DIC software.

4.1 *Vibrating Cantilever Beam Deformation Measurement*

The DIC technique was first validated by measuring the displacement of a vibrating cantilever beam, as shown in Fig. 5. A close up of the cantilever with the speckle pattern painted on the beam is shown in Fig. 6. The two cameras were focused on an aluminum cantilever beam that was excited by piezoelectric sheet actuators bonded near the root. The beam was excited at its second natural frequency, which was approximately 15 Hz. The cantilever beam was illuminated by a 1 kW halogen lamp, and the camera shutter speed was set fast enough to acquire an image without blur, but slow enough to ensure sufficient intensity and contrast of the captured image. This set of measurements required triggering the image acquisition at the same frequency as the beam vibration, followed by phase averaging the results over a number of cycles.

Images of the cantilever beam at rest were taken as the undeformed reference condition. A laser distance sensor (LDS) was used to verify the transverse displacement of the beam as measured by the DIC technique. Because the cameras have a fixed zoom factor, the field of view was adjusted by moving the cameras closer to, or farther away from the target. As the entire beam did not fit inside the camera field of view, it was necessary to combine multiple data sets in order to get the full view. This was accomplished by shifting the cameras along the beam span, making several measurements at each location, and then superimposing the results to recreate the deflection over the entire beam span.

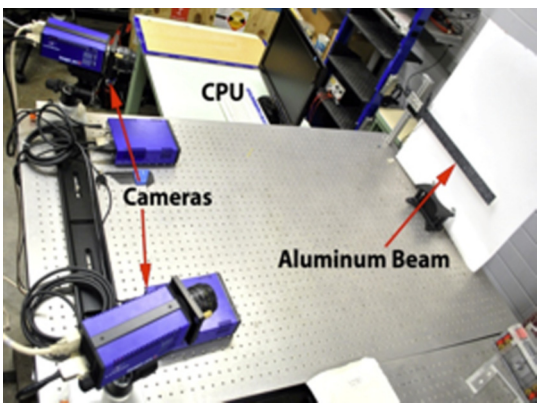

Fig. 5 Validation of DIC technique on vibrating cantilever beam.

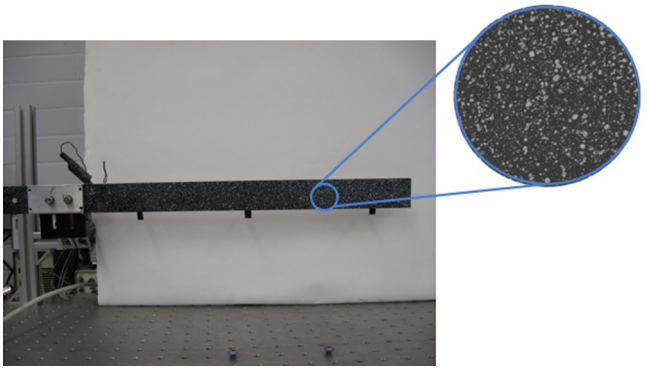

Fig. 6 Close-up of speckle pattern on vibrating cantilever beam.

4.2 *Rotating Blade Deformation Measurement*

After the DIC measurement methodology was validated on the cantilevered beam setup, the study progressed to measurements of rotating blade deformation. Experiments were performed on two rotors with different diameters (24 and 39 in.) and different rotor hubs. These reduced-scale helicopter rotor tests were performed on two separate hover test stands, both of which were designed and built in-house.

4.2.1 *Two-bladed rigid rotor*

A 24 in. diameter, two-bladed rotor with a rigid hub was mounted on a test stand driven by a brushless out-runner DC motor (Hacker A50 16S). The blades were commercially available, remotely controlled hobby helicopter blades, with a NACA 0012 airfoil section and constant chord of 1 in. Three high-speed digital servos operate a swash-plate assembly, allowing for precise control of the rotor collective and cyclic pitch angles. A magnetic pickup is used to measure the rotational speed and also provides a trigger for the DIC system and a strobe light. The assembly is mounted on a six component load cell (ATI Mini40E) which can measure up to 5 lbs of thrust. Data was acquired by a National Instruments CompactDAQ with a custom Labview virtual instrument. Measurements were made at two rotational speeds (1500 and 1800 RPM) and five collective pitch angles (3.56, 6.07, 8.55, 12.27, and 14.76 deg). The entire blade could not fit inside the field of view of the cameras and hence the results for this experiment are offset by approximately 3.5 in. from the root of the blade.

4.2.2 *Four-bladed articulated rotor*

The 39 in. diameter rotor blades were tested on a larger test stand, having a four-bladed articulated hub and driven by a brushless DC motor (Hacker A150-8). The blades were commercially available, remotely controlled hobby helicopter blades, with a NACA 0014 airfoil section and constant chord of 2.05 in. A servo-controlled swash-plate assembly was used to precisely control the rotor collective and cyclic pitch. It was not possible to directly measure the rotor forces because this test stand did not have a load cell. The full-field blade deformation was measured at three rotational speeds (400, 900, and 1200 RPM), 50 images per set, and two collective pitch angles (3.5 and 8 deg). The rotor test stand is shown in Fig. 7, and the calibration process is shown in Fig. 8. The entire blade could not fit inside the field of

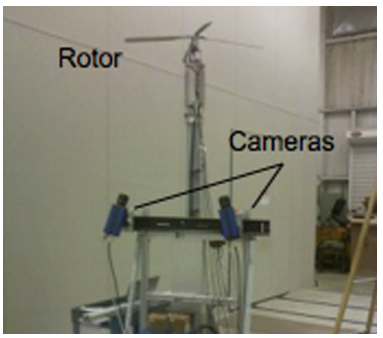

Fig. 7 Rotor test stand with 39 in. diameter rotor and cameras installed.

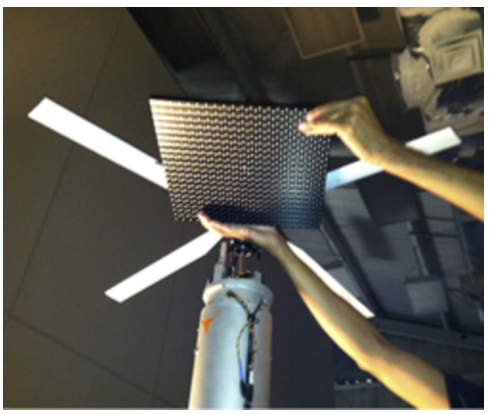

Fig. 8 Calibration of camera setup for DIC using a target of known geometry.

view of the cameras and hence the results for this experiment are offset by approximately 7 in. from the root of the blade.

In addition to the difference in size, note that there is a major difference in the rotor hubs between the two test stands. The smaller rotor has a rigid hub, which means that the rotor blades can only undergo elastic bending. Torsion is a combination of pitch angle at the blade root and elastic twist. The larger rotor has an articulated hub, which means that the rotor blades can undergo flapping (rigid body rotation about a flapping hinge located at the blade root) as well as elastic bending. In this case, torsion is a combination of rigid pitch angle and elastic twist.

For the rotor experiments, the magnetic pickup was used to trigger image acquisition at a specific rotor azimuthal position. Phase delays were introduced in the trigger signal to capture images at different azimuthal angles. Due to the higher frequency of the rotor blades (compared to the vibrating cantilever beam), the camera shutter was kept open for a set time period while a shorter duration strobe light was triggered by the magnetic pickup. In this way, higher speed image acquisition could be performed while ensuring blur-free images of adequate intensity and contrast. Because the cameras were limited to a continuous acquisition frequency of 15 Hz, which was slower than the rotational speed of the rotor, they were unable to capture images at every rotor revolution. Some fluctuations in the blade position was observed between frames due to slight variations in the rotational speed of the rotor. However, these errors were minimized by the phase averaging technique.

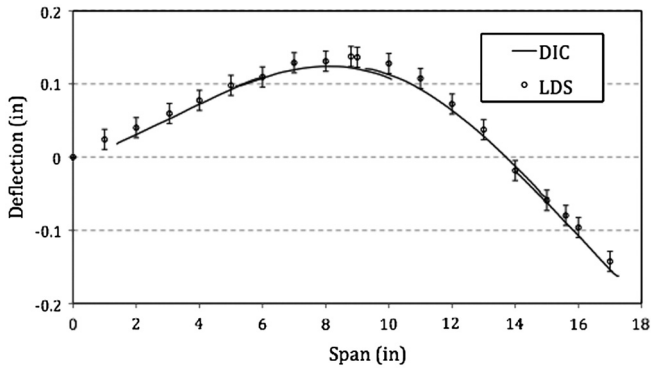

Fig. 9 Comparison of beam transverse deflection measured by DIC and LDS.

Images of the blades at a low rotational speed (around 200 RPM) and zero pitch angle were taken as the undeformed reference. All blade deformations are calculated with respect to this reference. Because of the low rotational speed and zero pitch angle, the reference condition approximated an undeformed rotor blade located perpendicular to the rotor shaft.

5 Error Analysis

For the result to be meaningful, it is essential to examine the sources of errors and their contributions to the measurement process. There have been several works that have specifically dealt with the error estimation.[21,23] Our error analysis is based on the software used in processing the results, wherein the dominant source of error in the DIC technique is related to the definition of the pixel group size. During the surface height calculation step, it is necessary to define an interrogation window which will determine the distance between neighboring vectors. It is possible to define these windows such that they overlap. The precision of the vectors depends on the size of this interrogation window and the amount by which each window overlaps. The distance between two neighboring vectors, or the vector grid, is determined by

$$g = \frac{\text{Interrogation window size}}{100/(100 - \%\text{overlap})}. \quad (1)$$

For example, an interrogation window size of 32×32 pixels with 50% overlap will have a vector grid of 16 pixels. The accuracy depends largely on the interrogation window size, but also on the zoom factor of the cameras, the type of lens used, and the distance to the test article.[22] Typical 3-D vector accuracy ranges from 0.01 to 0.1 pixels with larger vector grids being more accurate. The errors

Table 1 Spatial resolution and estimated accuracy of DIC deformation measurements.

Experiment	Calibration factor (pixel/in)	Spatial resolution)		Accuracy	
		(in.)	(%R)	(in.)	(%R)
Vibrating beam	243.4	0.066	0.369	2.05E-04	0.0012
Rotor blades	198.7	0.081	0.822	2.52E-04	0.0026

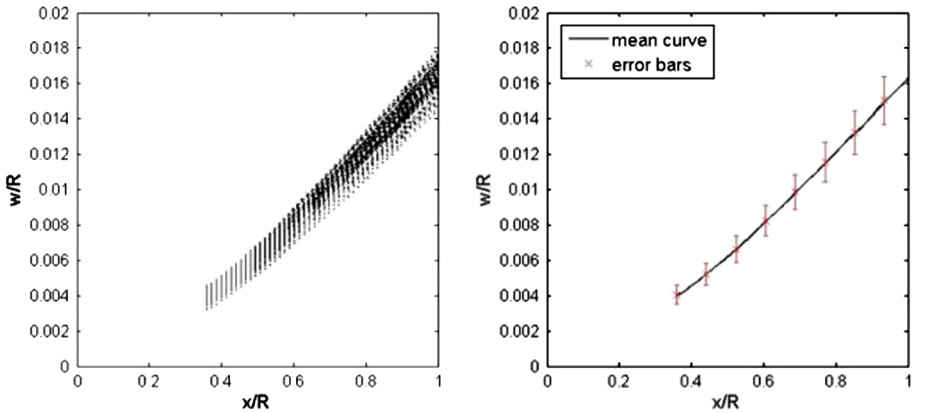

Fig. 10 Measured deflection for 24 in. diameter rotor, 1500 RPM at 8.5 deg collective pitch angle.

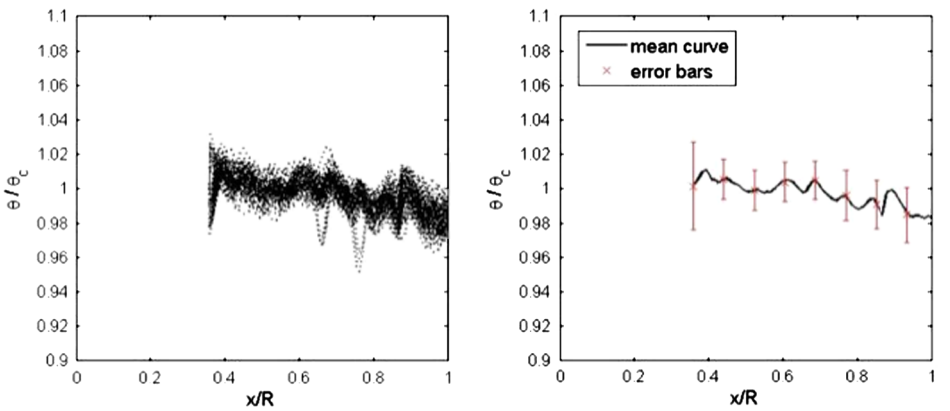

Fig. 11 Measured blade pitch angle as a function of spanwise location, 24 in. diameter rotor, 1500 RPM at 8.5 deg collective pitch angle.

propagate when calculating strain, and the absolute error increases with greater deformation. The error in the strain values is greater for smaller interrogation windows, and detecting strain smaller than 1% to suitable accuracy cannot be done with smaller vector grids as the noise level approaches the order of magnitude of the strain to be measured.[22] However, larger interrogation windows reduce the spatial resolution and may not resolve local discontinuities in the strain field. So, it is important to find a middle ground that offers the best spatial resolution obtainable while still capable of suitably accurate strain calculation. Table 1 gives the calibration factor, spatial resolution and accuracy obtained for the various experiments conducted. It can be seen that the accuracy is much better than required for structural dynamic analysis.

6 Results and Discussion

The transverse displacement of the cantilever beam was measured using DIC and was correlated with measurements from a laser LDS. A comparison between the results of both techniques is shown in Fig. 9. Because the beam motion was predominantly out of plane, a fixed mask was used that deformed with the structure. A 32×32 pixel interrogation window with 50% overlap was used in the surface height calculation. Since the entire beam could not fit inside the field of view of the cameras, it was split into two segments and the measurements were merged/stitched using a common identifying mark on the beam. Note that the DIC measurements lie within the error bars of the LDS measurements, verifying the accuracy of the DIC technique on a moving target.

Measurements on the 24 in. diameter rotor blades focused on the outer 60% of the blade span due to the large aspect ratio of the blades. The bending deflection shape was

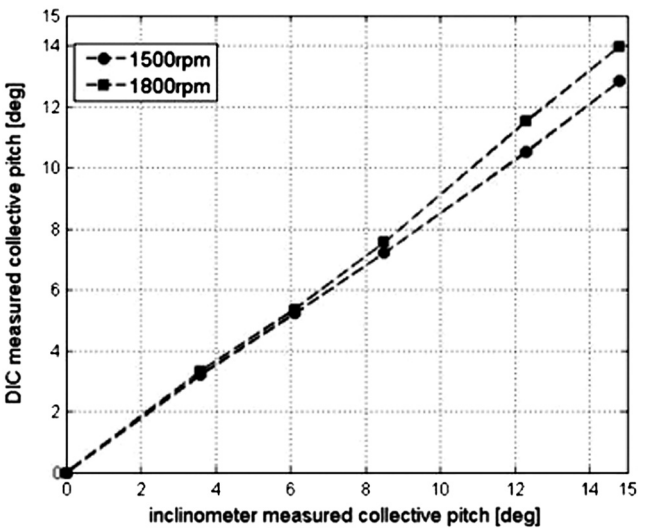

Fig. 12 Comparison of collective pitch measured by inclinometer and extracted from DIC data.

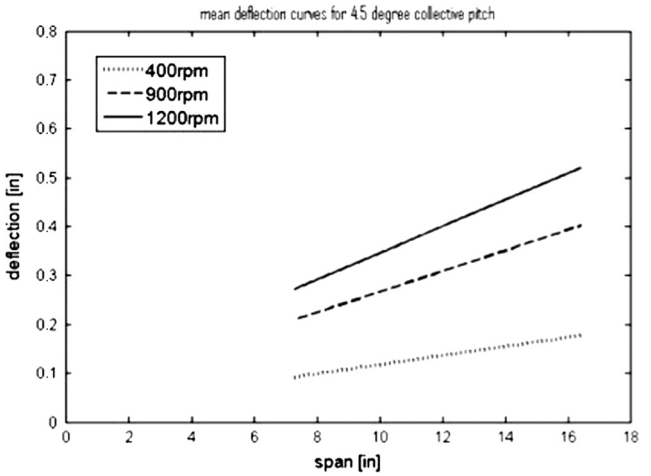

Fig. 13 Mean transverse deflection for 39 in. diameter rotor blades at 4.5 deg collective pitch.

automatically extracted from the blade quarter-chord line, and the slope of the chord line was used to find the twist angle at each point along the span. Figure 10 shows the measured deflection from all the images taken of the 24 in. diameter rotor blade at 1500 RPM and 8.5 deg collective pitch. The transverse displacement (w) on the y-axis and the spanwise location (x) on the x-axis are shown as a fraction of the rotor radius (R). Because the blades are relatively stiff and are attached to a rigid hub, the transverse displacements are small. Most of the deformation occurs towards the blade root. The spread of the measurements is due to slight variations in the rotational speed of the rotor, which causes variations in the position of the image of the rotor blade.

Figure 11 shows the blade pitch angle as a function of spanwise location for the 24 in. diameter rotor blade at 1500 RPM and 8.5 deg collective pitch. The blade pitch (θ) is shown as a fraction of the root pitch (θ_c). Because the blades are stiff in torsion, the twist deformation along the blade is very small. The slight scattering of pitch values at each radial position was also observed by Olson et al.[11] in their calculation of pitch on a full-scale UH-60A rotor blade. It was concluded that this variation was possibly due to imperfections in the airfoil lower surface geometry. The

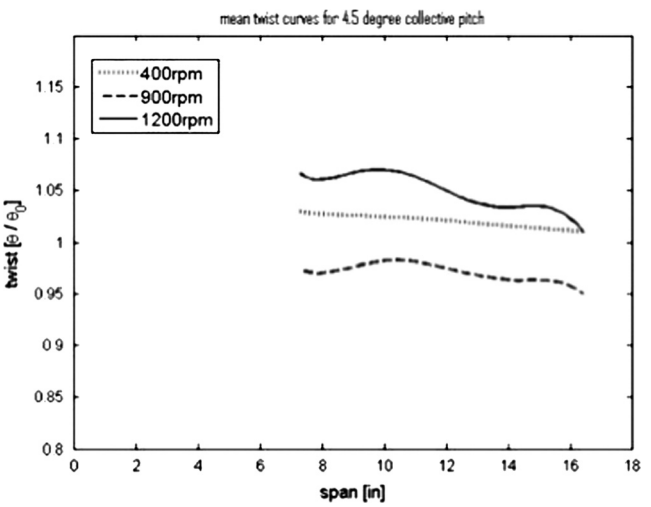

Fig. 14 Spanwise variation of blade pitch, 39 in. diameter rotor blades at 4.5 deg collective.

error associated with twist is further propagated because twist is a derived quantity from multiple displacements. Figure 12 shows a comparison of collective pitch angles as measured by an inclinometer and extracted from DIC data. It is seen that the maximum error, at higher collective pitch angles, is around 6%.

For the 39 in. diameter rotor, the transverse deflection curves are linear due to the flapping hinge near the blade root (see Fig. 13). Although the blades are relatively rigid in twist, the aerodynamic pitching moment creates a small negative twist along the span, as can be seen in Fig. 14. As discussed previously, the slight nonlinear variation of pitch values at each radial position is due to imperfections in the airfoil lower surface geometry which was also observed by Olson et al.[11] in their calculation of pitch on a full-scale UH-60A rotor blade.

7 Concluding Remarks

The DIC technique has proven to be a viable method for obtaining deflection characteristics of reduced-scale rotating helicopter blades. Instantaneous snapshots of periodic motion can be obtained by synchronizing the digital cameras with a trigger signal coordinated with the motion. This synchronization can also be used to phase average the results for increased accuracy. The technique was validated on a vibrating cantilever beam and the DIC measurements were within the experimental error bounds of a LDS. The technique can easily be extended to measured the deflection of rotor blades in rotation. Measurements of rotor blade deformation can be made at high rotational speeds without the need for high-speed digital cameras. Flapping and pitching shapes are fairly easily extracted from the vector deformation field. The measured transverse deflection and blade pitch follow expected trends with collective pitch and rotational speed variation. The collective pitch angle measured using DIC correlates with the measurements using an inclinometer with an error of less than 6%.

It has been demonstrated that DIC techniques could be used to measure deformations of rotating blades with sufficient accuracy for aerodynamic and dynamic analyses. The DIC technique can extend the range of deflection measurements from tens of micrometers, using coherent speckles as in ESPI, to the order of 10 mm without the need for coherent speckles. Future efforts will involve extending the technique to larger diameter rotors with the goal of eliminating on-blade strain sensors in wind tunnel and flight tests.

References

1. A. Datta and I. Chopra, "Validation of structural and aerodynamic modeling using UH-60A airloads program data," *J. Am. Helicopter Soc.* **51**(1), 43–58 (2006).
2. R. Steijl, G. N. Barakos, and K. J. Badcock, "Computational study of the advancing-side lift-phase problem," *J. Aircraft* **45**(1), 246–257 (2008).
3. T. Schmidt, J. Tyson, and K. Galanulis, "Full-field dynamic displacement and strain measurement using advanced 3-D image correlation photogrammetry: part 1," *Exp. Tech.* **27**(3), 47–50 (2003).
4. R. S. Sirohi, *Optical Methods of Measurement: Whole-field Techniques*, 2nd ed., CRC Press, Taylor and Francis Group, Boca Raton, FL (2009).
5. G. Cloud, *Optical Methods of Engineering Analysis*, Cambridge University Press, New York (1995).
6. D. C. Williams, *Optical Methods in Engineering Metrology*, Chapman and Hall, London (1993).
7. J. Tyson, "Noncontact full-field strain measurement with 3-D ESPI," *Sensors* **17**(5), 62–70 (2000).

8. M. Anguiano-Morales et al., "Micro-and macro deformation measurement by extension of digital correlation technique," *Optik* **122**(18), 1642–1645 (2011).
9. G. A. Fleming and S. Gorton, "Measurement of rotorcraft blade deformation using projection moire interferometry," *Proc. SPIE* **3441**, 514–527 (1998).
10. E. J. Pryputniewicz, G. A. Flemming, and R. J. Pryputniewicz, "Experimental characterization of vibrations of a NASA active twist rotor blade," in *Proc. of the IMAC-XXII: Conf. & Exposition on Structural Dynamics*, Society for Experimental Mechanics, Inc., Bethel, CT (2004).
11. L. Olson et al., "Blade deflection measurements of a full-scale UH-60A rotor system," *American Helicopter Society Aeromechanics Specialist's Conference*, San Francisco, California (20–22 January 2010).
12. S. Robson and H. B. Setan, "The dynamic digital photogrammetric measurement and visualization of 21 m wind turbine rotor blade udergoing structural analysis," *Int. Arch. Photogram. Rem. Sens. Vienna* **XXXI**(Pt. B5), 493–498 (1996).
13. T. Liu et al., "Photogrammetry applied to wind tunnel testing," *AIAA J.* **38**(6), 964–971 (2000).
14. A. W. Burner and T. Liu, "Videogrammetric model deformation measurement technique," *J. Aircraft* **38** (4), 745–754 (2001).
15. T. C. Chu, W. F. Ranson, and M. A. Sutton, "Applications of digital image correlation techniques to experimental mechanics," *Exp. Mech.* **25**(3), 232–244 (1985).
16. T. Schmidt, J. Tyson, and K. Galanulis, "Full-field dynamic displacement and strain measurement – specific examples using advanced 3-D image correlation photogrammetry, part 2," *Exp. Tech.* **27**(4), 22–26 (2003).
17. P. Wu et al., "Digital image correlation techniques for full-field displacement measurements of micro air vehicle flapping wings," *Exp. Tech.* **33**(6), 53–58 (2009).
18. J. Tyson, T. Schmidt, and K. Galanulis, "Advanced photogrammetry for robust deformation and strain measurement," *SEM 2002 Annual Conf.*, SEM, Milwaukee, WI (2002).
19. Z. L. Kahn-Jetter and T. C. Chu, "Three-dimensional displacement measurements using digital image correlation and photogrammic analysis," *Exp. Mech.* **30**, 10–16 (1990).
20. S. R. McNeill et al., "Measurement of surface profile using digital image correlation," *Exp. Mech.* **37**(1), 13–20 (1997).
21. T. Siebert et al., "High speed digital image correlation error estimations and applications," *Opt. Eng.* **46**, 051004 (2007).
22. La Vision, DaVis StrainMaster 3-D, Software Package, Ver 7.2, Göttingen, Germany, (January 2010).
23. H. Haddadi and S. Belhabib, "Use of rigid-body motion for the investigation and estimation of the measurement errors related to digital image correlation technique," *Opt. Laser Eng.* **46**(2), 185–196 (2008).

Biographies and photographs of the authors not available.